Strojniški vestnik - Journal of Mechanical Engineering 70(2024)3-4, 181-193
© 2024 The Authors. CC BY 4.0 Int. Licensee: SV-JME
DOI:10.5545/sv-jme.2023.825
Original Scientific Paper
Received for review: 2023-10-09
Received revised form: 2023-12-19
Accepted for publication: 2023-12-23

Nonlinear Free Vibration Analysis of Functionally Graded Porous Conical Shells Reinforced with Graphene Nanoplatelets

Xiaolin Huang – Nengguo Wei – Chengzhe Wang – Xuejing Zhang*
Guilin University of Electronic Technology, School of Architecture and Transportation Engineering, China

The nonlinear vibration analysis of functionally graded reinforced with graphene platelet (FG-GRC) porous truncated conical shells surrounded by the Winkler-Pasternak elastic foundation is presented in this paper. An improved model for evaluating the material properties of porous composites is proposed. Three types of porous distribution and three patterns of graphene nanoplatelets (GPLs) dispersion are estimated. Coupled with the effect of the Winkler-Pasternak elastic foundation, the nonlinear governing equations are developed by using the Hamilton principle. The Galerkin integrated technique is employed to obtain the linear and nonlinear frequencies of the shells. After the present method is validated, the effects of the pores, GPLs, the Winkler-Pasternak foundation, and the semi-vertex are investigated in detail. The results show that the linear frequency can be raised by increasing the values of the mass volume of the GPL and foundation parameters. In contrast, the ratio of nonlinear to linear frequency declines as the mass volume of the GPLs and foundation parameters rises. Furthermore, it is found that the minimum ratio of nonlinear to linear frequency can be obtained as the semi-vertex angle is about 55°, and the effect of porosity distribution on the linear and linear frequencies might be neglected.

Keywords: nonlinear vibration, truncated conical shell, graphene nanoplatelet, porous materials, elastic foundation

Highlights

- *A new model for estimating the material properties of FG-GRCs is presented.*
- *The nonlinear vibrational equations for FG-GRCs conical shells are built.*
- *The formulations for the linear and nonlinear frequency of FG-GRCs conical shells are presented.*

0 INTRODUCTION

Because the nonlinear dynamic behaviour of structures inevitably appears in engineering applications, the nonlinear characteristics of the structures have attracted the attention of many researchers. For example, Lu et al. [1] and [2] and Hao et al. [3] developed a novel model to analyse the nonlinear vibration of isolation systems with a high-static-low-dynamic stiffness. They validated the analytical results by using direct time integration and experiments. The inherent vulnerability of nonlinear vehicle platoons was studied by Wang et al. [4]. They proposed a vibration-theoretic approach to compute the platoon's resonance frequency. Zhou et al. [5] presented a high-order nonlinear friction model to investigate the nonlinear hysteresis characteristics of metal rubbers. They found that the nonlinear friction hysteresis dynamic model has a high prediction accuracy and signal-to-noise ratio. Yang and Kai [6] built the nonlinear coupled Schrodinger equation in fibre gratings, and the periodic solution was presented. For porous composite plates reinforced with graphene platelets, Huang et al. [7] presented a two-step perturbation technique to analyse the nonlinear vibration of the plates. In their studies, the effects of the pores, graphene platelets, and elastic foundations on the nonlinear to linear frequency ratio were discussed in detail.

Due to the advantages of withstanding severe high temperatures while maintaining structural integrity, functionally graded materials (FGMs) are widely used in engineering fields such as aerospace, nuclear, mechanical, and civil engineering. The nonlinear static and dynamic characteristics of FGM shell structures have gained much attention. Chan et al. [8] to [10] studied the nonlinear buckling and vibration of FGM truncated conical shells, and Duc et al. [11] and Vuong et al. [12] investigated the nonlinear stability of FGM toroidal shells.

Applying the concept of FGMs, a new type of functionally graded nanocomposites, in which the carbonaceous nanofilters such as graphene platelets (GPLs) and carbon nanotubes (CNTs), are gradually distributed in the thickness direction of the polymeric matrix, has been developed. Because nanocomposites are one of the most promising materials in composite structures, research work has been devoted to examining the linear vibration of functionally graded truncated conical shells reinforced by GPLs and CNTs. Wang et al. [13] studied the free vibration of the composite conical shells reinforced with GPLs. They found that the fundamental frequency is greatly affected by the distribution patterns of GPLs. Afshari [14] and [15] examined the vibration characteristics

*Corr. Author's Address: Guilin University of Electronic Technology, Jinji Road 1#, Guilin, China,pingguotree4426@163.com

of truncated conical shells reinforced with graphene nanoplatelets and discussed the influences of the boundary conditions and constant angular velocity on the natural frequencies. For the joined conical-conical shells made of epoxy-enriched with graphene nanoplatelets, Damercheloo et al. [16] studied free vibration and examined the influences of the boundary conditions, the length-to-small radius ratio, and semi-vertex angle in two shell segments. Using the finite element method in conjunction with a higher-order shear deformation theory, Singha et al. [17] investigated the free vibration behaviour of rotating pre-twisted sandwich conical shell panels with functionally graded graphene-reinforced composite face sheets and homogenous cores in a uniform thermal environment. In their studies, the influence of graphene distribution patterns on the fundamental frequencies is discussed with an emphasis on triggering parameters like pre-twist angle, cone length-to-thickness ratio, core-to-face sheets thickness ratio, and dimensionless rotational speed. Adab et al. [18] and [19] presented a vibrational analysis on truncated conical sandwich microshells. For the vibration behaviour of the composite conical shell reinforced with CNTs, Yousef et al. [20] and [21] investigated the effect of CNTs agglomeration on the vibration characteristics of three-phase CNT/polymer/fibre laminated truncated conical shells. The results show that the subjoining of CNTs leads to a remarkable rise in the natural frequency. Employing the first-order shear deformation theory and the Eshelby-Mori-Tanaka scheme along with the rule of mixture, Afshari and Amirabadi [22] conducted the free vibration analysis of rotating truncated conical shells reinforced with CNTs and the effects of different parameters on the forward and backward frequencies of the shells are investigated. Moreover, the aeroelastic stability of polymeric truncated conical shells reinforced with CNTs and under supersonic fluid flow was studied by Afshari et al. [23]. However, the published literature on the nonlinear vibrations of functionally graded graphene-reinforced composite (FG-GRC) plates and conical shells is limited. Using the 2-D differential quadrature method, arc-length continuation technique, and harmonic balance technique, Jamalabadi et al. [24] studied the nonlinear vibration of FG-GRC truncated conical shells and investigated the effects of the mass volume and distribution of the GPLs, semi-vertex, and foundation parameters on the ratio of linear to nonlinear frequency. They found that the rising valve of the GPL mass volume can raise the linear frequency. In contrast, the ratio of the nonlinear to linear frequency declines. Using the variational differential quadrature and finite element method, Ansari et al. [25] investigated the nonlinear vibration characteristics of FG-GRC conical panels with arbitrary-shaped cutouts. The results show that the natural frequency rises as the weight fraction of the GPLs increases. Yang et al. [26] employed the Galerkin and harmonic balance methods to obtain the nonlinear frequencies of FG-GRC conical shells and studied the periodic and chaotic motions. To investigate the nonlinear dynamic characteristics of FG-GRC conical shells, Wang et al. [27] employed the Galerkin method and fourth-order Runge-Kutta technique to obtain the frequency response. They found that both the mass volume and distribution of GPLs significantly affect the resonance response of the shells. Ding and She [28] obtained the nonlinear dynamic response of FG-GRC truncated conical shells and discussed the effects of the mass fraction of the GPLs, geometrical parameters, and the position of the external load on the response. Additionally, Bidgoli and Arefi [29] presented the nonlinear vibration analysis of sandwich plates with graphene nanoplatelet-reinforced face sheets. They found that the nonlinear to linear frequency ratio can be affected by the weight fraction and geometric parameters of graphene nanoplatelets.

In the literature above, the conical shells were regarded as the perfect structures without pores. However, internal pores may appear inside composite materials [30]. Thus, it is necessary to investigate the effect of internal pores on the dynamic behaviour of porous structures. Some researchers studied the vibration characteristics of porous isotropic [31] and [32], sandwich [33] and [34]. For the functionally graded porous (FGP) truncated conical panels with piezoelectric actuators in thermal environments, Chan et al. [35] investigated the nonlinear dynamic response and free vibration. In their studies, the effect of the porosity distribution on the natural frequency and the deflection amplitudes were discussed. Considering the two types of porosity distribution, the buckling and vibration of sigmoid functionally graded material shells were studied by Huang et al. [36]. The results show both the porosity volume fraction and distribution have significant effects on the buckling pressures and lowest frequency. Nevertheless, little work has been done for the porous truncated conical shells reinforced by nano filters [37]. Bahhadini et al. [38] and Yan et al. [39] studied the linear vibration of porous FG-GRC nanocomposite sandwich conical shells and found that the natural frequencies were increased with the rising material length-scale parameter and porosity coefficient. The

vibration behaviour of porous sandwich truncated conical shells with FG face sheets and a saturated FGP core was studied by Rahmani et al. [40] and Esfahani et al. [41]. The effect of internal pores on the natural frequency was also discussed in detail. Applying the isogeometric analysis, Le et al. [42] obtained the three-dimensional solution of the free vibration and buckling for functionally graded porous-cellular conical shells. Sobhani et al. [43] studied the vibrational behaviour of porous nanocomposite joined hemispherical-cylindrical-conical shells and examined the effects of the porosity distributions and geometric properties. The results revealed that the natural frequency inclines with the increase of the porosity factor. Additionally, the free vibration of FG-joined conical-cylindrical shells reinforced with graphene nanoplatelets was investigated by Kiarasi et al. [44]. It was found that the volume fraction and distributions of the internal pores have an insignificant impact on the natural frequencies of FG-GRC porous conical shells.

Unlike the Winkler elastic foundation model, the Winkler-Pasternak model incorporates the shear interaction between structures and foundations and has been widely used to examine the dynamic behaviour of FGM-truncated conical shells [45] to [47]. However, the model was used less to investigate the vibration of FG-GRC conical shells. Safarpour et al. [48] studied the free vibration of perfect and imperfect FG-GRC conical shells resting on Pasternak foundations. Their results show that the effect of the elastic foundation becomes more dominant as the foundation parameters increase. Eyvazian et al. [49] computed the natural frequencies and the corresponding mode shapes of FG-GRC conical panels and discussed the influences of boundary conditions, GPLs volume fraction, and foundation parameters. Furthermore, the frequency responses of rotating two-directional FG-GPLs conical shells on elastic foundations were presented by Amirabadi et al. [50]. They found that the increasing value of the GPL mass fraction can raise the natural frequency. The pattern of GPLs scattering near the inner surface has a higher effect on the frequency.

As reviewed above, the published literature on the free vibration of FG-GRC porous truncated conical shells remains limited. Most of the open literature focused on the case of the linear problem. The model used for evaluating the material properties of porous nanocomposites was based on the three assumptions about Young's elastic modulus, shear modulus, and mass density, which is too complicated. Hence, the present work attempts to solve these problems, that is, to propose an improved model for estimating the material properties and present the analytical solution for the nonlinear free vibration of FG-GRC porous truncated shells. Also, the effects of the internal pores, GPL, and elastic foundation on the linear and nonlinear frequencies are investigated.

1 A POROUS FG-GPLS TRUNCATED CONICAL SHELL

As shown in Fig. 1, a porous FG-GPLs truncated conical shell surrounded by Winkler-Pasternak elastic medium is considered. The curvilinear coordinate system (x, θ, z) is located on the middle surface of the shell. s_1 and s_2 are the distances from the vertex to the small and large ends, respectively. L, h and α denote the length, thickness, and semi-vertex of the shell.

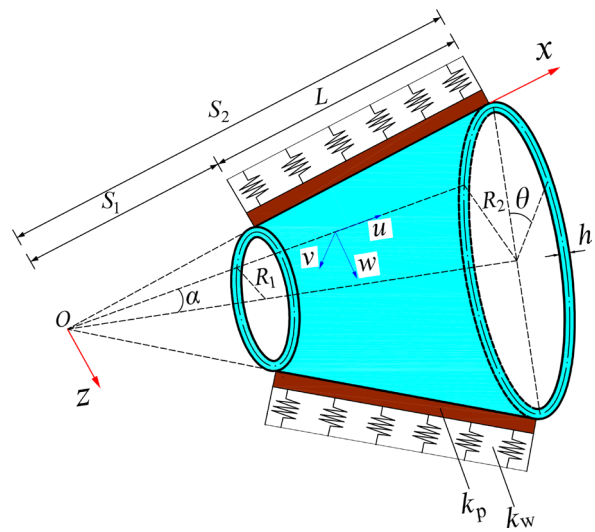

Fig. 1. *A FG-GPLs truncated conical shell surrounded by a Winkler-Pasternak elastic foundation*

Three types of porous distribution in the thickness direction, denoted by P-1, P-2, and P-3, are taken into account, as depicted in Fig. 2.

It is assumed all the internal pores are tiny and the total volume fraction of the pores is small. Unlike other models for evaluating the material properties [30] and [39], in which Young's modulus, shear modulus, and mass density need to be assumed, the present model is based on the following assumption about the volume fraction $V_P(z)$ of the internal pores:

$$V_P(z) = e_0 \cos\left(\frac{\pi z}{h}\right), \quad \text{(P-1)}$$

$$V_P(z) = e_0 \cos\left(\frac{\pi z}{2h} + \frac{\pi}{4}\right), \quad \text{(P-2)}$$

$$V_P(z) = e_0, \quad \text{(P-3)} \qquad (1)$$

here, e_0 denotes the porosity coefficient. Young's elastic modulus $E(z)$ and mass density $\rho(z)$ for various porosity distributions can be expressed as [39].

$$E(z) = E_1\left(1 - V_P(z)\right),$$
$$\rho(z) = \rho_1\left(1 - \frac{e_m}{e_0}V_P(z)\right), \quad (2)$$

where E_1 and ρ_1 denote the maximum values of Young's modulus and mass density, and e_m is the mass coefficients. Furthermore, the coefficients e_0, e_m and the Poisson ratio $\mu(z)$ are calculated as follows [39]:

$$e_\mathrm{m} = \frac{1.121e_0[1-\sqrt[2,3]{1-V_P(z)}]}{V_P(z)},$$
$$\mu(z) = 0.221p + \mu_1(0.342p^2 - 1.21p + 1.0),$$
$$p = 1.121(1-\sqrt[2,3]{1-V_P(z)}), \quad (3)$$

in which μ_1 is the Poisson ratio of the composite without pores, and p is the coefficient of the Poisson ratio.

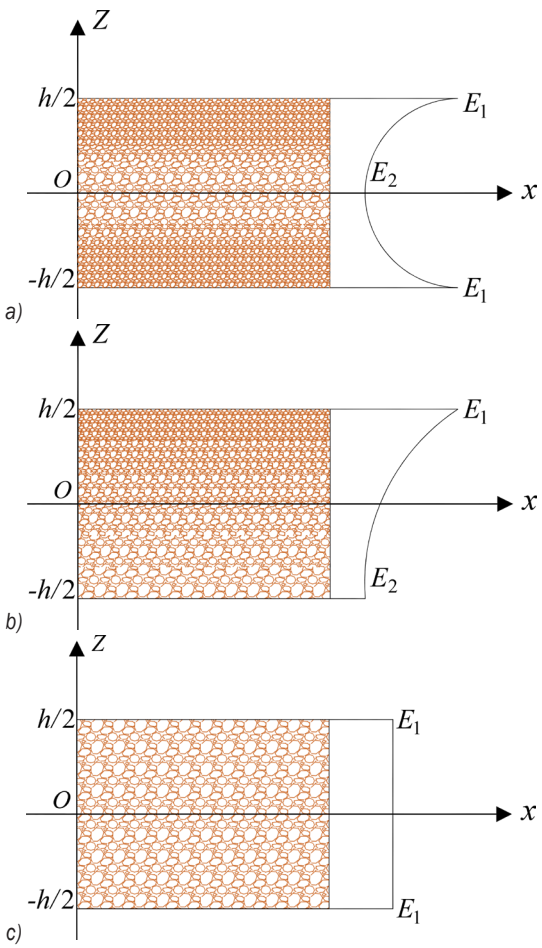

Fig. 2. *Three types of porosity distribution: a) symmetric distribution (P-1), b) asymmetric distribution (P-2), and c) even distribution (P-3)*

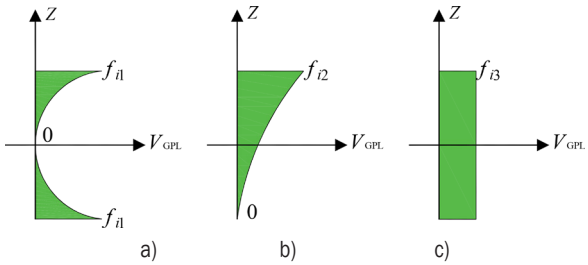

Fig. 3. *Three patterns of GPLs dispersion: a) symmetric distribution (G-1), b) asymmetric distribution (G-2), and c) even distribution (G-3)*

It is noted that the present model in Eqs. (1) to (3) can be used not only for FG-GRCs but also for other composites in which the foam metal is the matrix.

In the present study, three patterns of GPL dispersion, denoted by G-1, G-2, and G-3, are considered, as shown in Fig. 3. The volume fractions $V_{GPL}(z)$ for the three patterns are expressed as follows [43]:

$$V_{GPL}(z) = f_{i1}\left[1 - \cos\left(\frac{\pi z}{h}\right)\right], \quad (G-1)$$
$$V_{GPL}(z) = f_{i2}\left[1 - \cos\left(\frac{\pi z}{2h} + \frac{\pi}{4}\right)\right], \quad (G-2)$$
$$V_{GPL}(z) = f_{i3}, \quad (G-3) \quad (4)$$

where f_{i1}, f_{i2} and f_{i3} are the maximum values of various GPL distributions, calculated by [39]:

$$\frac{W_{GPL}}{W_{GPL} + (\rho_{GPL}/\rho_\mathrm{m})(1-W_{GPL})}\int_{-h/2}^{h/2}\left[1 - \frac{e_\mathrm{m}}{e_0}V_P(z)\right]dz$$
$$= \int_{-h/2}^{h/2} V_{GPL}(z)\left[1 - \frac{e_\mathrm{m}}{e_0}V_P(z)\right]dz. \quad (5)$$

In Eqs. (2) and (3), E_1, ρ_1, and μ_1 can be determined by using the Halpin-Tsai micromechanics model and the rule of the mixture as follows [39]:

$$E_1 = \frac{3}{8}\left(\frac{1+\xi_\mathrm{a}\eta_\mathrm{a}V_{GPL}}{1-\eta_\mathrm{a}V_{GPL}}\right)E_\mathrm{m} + \frac{3}{8}\left(\frac{1+\xi_\mathrm{b}\eta_\mathrm{b}V_{GPL}}{1-\eta_\mathrm{b}V_{GPL}}\right)E_\mathrm{m}, \quad (6)$$
$$\rho_1(z) = V_{GPL}(z)\rho_{GPL} + \left[1 - V_{GPL}(z)\right]\rho_\mathrm{m}, \quad (7)$$
$$\mu_1(z) = V_{GPL}(z)\mu_{GPL} + \left[1 - V_{GPL}(z)\right]\mu_\mathrm{m}, \quad (8)$$

in which the geometric parameters of GPL ξ_a , ξ_b, η_a and η_b can be stated as

$$\xi_\mathrm{a} = \frac{2a_{GPL}}{h_{GPL}}, \qquad \xi_\mathrm{b} = \frac{2b_{GPL}}{h_{GPL}},$$
$$\eta_\mathrm{a} = \frac{E_{GPL}/E_\mathrm{m} - 1}{E_{GPL}/E_\mathrm{m} + \xi_\mathrm{a}}, \quad \eta_b = \frac{E_{GPL}/E_\mathbf{m} - 1}{E_{GPL}/E_\mathrm{m} + \xi_\mathrm{b}}, \quad (9)$$

here, E_{GPL}, ρ_{GPL} and μ_{GPL} denote the Young's modulus, mass density and Poisson ratio of GPL, and E_m, ρ_m and μ_m are the corresponding values of the matrix. a_{GPL}, b_{GPL} and h_{GPL} are the length, width, and thickness of the GPL.

2 FORMULATIONS

2.1 Governing Equations

It is assumed that the shell is thin and has a large deformation. According to the classic shell theory with the geometrical nonlinearity, the normal strains (ε_1, ε_2) and shear strain γ_{12} can be expressed as [51]

$$\varepsilon_1 = \varepsilon_1^0 + z\kappa_1, \quad \varepsilon_2 = \varepsilon_2^0 + z\kappa_2, \quad \gamma_{12} = \gamma_{12}^0 + 2z\kappa_{12}, \tag{10}$$

in which the strains $\left(\varepsilon_1^0, \varepsilon_2^0, \gamma_{12}^0\right)$, curvatures ($\kappa_1, \kappa_2$) and twist κ_{12} in the middle surface are defined by [51]

$$\begin{aligned}
\varepsilon_1^0 &= \frac{\partial u}{\partial x} + \frac{1}{2}\left(\frac{\partial u}{\partial x}\right)^2,\\
\varepsilon_2^0 &= \frac{1}{x\sin\alpha}\frac{\partial v}{\partial \theta} + \frac{u}{x} + \frac{w}{x}\cot\alpha + \frac{1}{2x^2\sin^2\alpha}\left(\frac{\partial w}{\partial \theta}\right)^2,\\
\gamma_{12}^0 &= \frac{1}{x\sin\alpha}\frac{\partial u}{\partial \theta} - \frac{v}{x} + \frac{v}{x}\cot\alpha + \frac{1}{x\sin\alpha}\frac{\partial w}{\partial x}\frac{\partial w}{\partial \theta},\\
\kappa_1 &= -\frac{\partial^2 w}{\partial x^2}, \qquad \kappa_2 = -\frac{1}{x^2\sin^2\alpha}\frac{\partial^2 w}{\partial \theta^2} - \frac{1}{x}\frac{\partial w}{\partial x},\\
\kappa_{12} &= -\frac{1}{x\sin\alpha}\frac{\partial^2 w}{\partial x \partial \theta} + \frac{1}{x^2}\frac{\partial w}{\partial \theta},
\end{aligned} \tag{11}$$

where u, v and w are the displacements along the directions of x, θ and z axes, respectively.

According to Hooke's law, the normal stresses σ_1 and σ_2, and the shear stress σ_{12} can be stated as [51]

$$\begin{pmatrix}\sigma_1\\ \sigma_2\\ \sigma_{12}\end{pmatrix} = \begin{bmatrix} Q_{11} & Q_{12} & 0\\ Q_{12} & Q_{22} & 0\\ 0 & 0 & Q_{66}\end{bmatrix}\begin{bmatrix}\varepsilon_1\\ \varepsilon_2\\ \gamma_{12}\end{bmatrix}. \tag{12}$$

Here, Q_{ij} ($i,j=1,2,6$) are the reduced stiffness coefficients, defined by [51]

$$\begin{aligned}
Q_{11} &= Q_{22} = \frac{E(z)}{1-\mu^2(z)}, \quad Q_{12} = \frac{\mu(z)E(z)}{1-\mu^2(z)},\\
Q_{66} &= \frac{E(z)}{2\left(1+\mu(z)\right)}.
\end{aligned} \tag{13}$$

The membrane forces (N_1, N_2, N_{12}) and moments (M_1, M_2, M_{12}) are expressed as [55]

$$\left[\left(N_1, N_2, N_{12}\right), \left(M_1, M_2, M_{12}\right)\right] = \int_{-h/2}^{h/2}\left[1, z\right]\left(\sigma_1, \sigma_2, \sigma_{12}\right)dz. \tag{14}$$

Substituting Eq. (12) into (14), the following equations can be obtained [51]:

$$\begin{aligned}
N_1 &= A_{11}\varepsilon_1^0 + A_{12}\varepsilon_2^0 + B_{11}\kappa_1 + B_{12}\kappa_2,\\
N_2 &= A_{12}\varepsilon_1^0 + A_{22}\varepsilon_2^0 + B_{12}\kappa_1 + B_{22}\kappa_2,\\
N_{12} &= A_{66}\gamma_{12}^0 + 2B_{66}\kappa_{12},\\
M_1 &= B_{11}\varepsilon_1^0 + B_{12}\varepsilon_2^0 + D_{11}\kappa_1 + D_{12}\kappa_2,\\
M_2 &= B_{12}\varepsilon_1^0 + B_{22}\varepsilon_2^0 + D_{12}\kappa_1 + D_{22}\kappa_2,\\
M_{12} &= B_{66}\gamma_{12}^0 + 2D_{66}\kappa_{12}.
\end{aligned} \tag{15}$$

The stiffness constants A_{ij}, B_{ij}, and D_{ij}, can be calculated by [51]

$$\left(A_{ij}, B_{ij}, D_{ij}\right) = \int_{-h/2}^{h/2} Q_{ij}\left(1, z, z^2\right)dz. \tag{16}$$

The interaction force between the Winkler-Pasternak medium and shell is assumed to be $F = k_w w - k_p \nabla^2 w$, in which k_w and k_p are the parameters of Winkler and Pasternak foundation, and ∇^2 is the Laplace operator. Using the Hamilton principle, the nonlinear dynamic Equilibrium equations of the conical shell surrounded by the Winkler-Pasternak medium can be derived as [51]:

$$\begin{aligned}
&x\frac{\partial N_1}{\partial x} + \frac{1}{\sin\alpha}\frac{\partial N_{12}}{\partial \theta} + N_1 - N_2 = \rho_t\frac{\partial^2 u}{\partial t^2},\\
&\frac{1}{\sin\alpha}\frac{\partial N_2}{\partial \theta} + x\frac{\partial N_{12}}{\partial x} + 2N_{12} = \rho_t\frac{\partial^2 v}{\partial t^2},\\
&x\frac{\partial^2 M_1}{\partial x^2} + 2\frac{\partial^2 M_1}{\partial x} + \frac{2}{\sin\alpha}\left(\frac{\partial^2 M_{12}}{\partial x \partial \theta} + \frac{1}{x}\frac{\partial M_{12}}{\partial \theta}\right)\\
&\quad + \frac{1}{x\sin^2\alpha}\frac{\partial^2 w}{\partial \theta^2} - \frac{\partial M_2}{\partial x} - N_2\cot\alpha\\
&\quad + \left(xN_1\frac{\partial w}{\partial x} + \frac{1}{\sin\alpha}N_{12}\frac{\partial w}{\partial \theta}\right)_{,x}\\
&\quad + \frac{1}{\sin\alpha}\left(xN_1\frac{\partial w}{\partial x} + \frac{1}{\sin\alpha}N_{12}\frac{\partial w}{\partial \theta}\right)_{,\theta}\\
&\quad - x\square w - x\square^2 w = x\rho_t\frac{\partial^2 w}{\partial t^2},
\end{aligned} \tag{17}$$

where the mass inertia is $\rho_t = \int_{-0.5h}^{0.5h}\rho(z)dz$.

Substituting Eqs. (11) and (15) into (17), the nonlinear vibrational equations of the shell can be derived as follows [51]:

$$L_{11}(u) + L_{12}(v) + L_{13}(w) + L_{14}(w) = \rho_t\frac{\partial^2 u}{\partial t^2}, \tag{18}$$

$$L_{21}(u) + L_{22}(v) + L_{23}(w) + L_{24}(w) = \rho_t\frac{\partial^2 v}{\partial t^2}, \tag{19}$$

$$L_{31}(u)+L_{32}(v)+L_{33}(w)+L_{34}(u,v,w)=x\rho_t\frac{\partial^2 w}{\partial t^2}, \quad (20)$$

where the linear operators L_{ij} $(i,j=1,2,3)$ have been given by Duc et al. [51]. The nonlinear operators L_{i4} $(i,j=1,2,3)$ are listed in Appendix. According to Volmir's assumption [26], the inertia forces $\rho_t\frac{\partial^2 u}{\partial t^2}$ and $\rho_t\frac{\partial^2 v}{\partial t^2}$ can be neglected.

2.2 The Solution of the Governing Equations

In this study, simply supported boundaries are considered. The boundary conditions are written as

$$v=w=0,\ N_1=0,\ M_1=M_{12}=0,\ \text{at } x=s_1,s_2. \quad (21)$$

In the present case, the asymmetric solution is taken into account. The solution satisfying the boundary conditions is assumed to be [51]

$$u=u_{mn}(t)\cos\frac{m\pi(x-s_1)}{L}\sin\left(\frac{n\theta}{2}\right),$$
$$v=v_{mn}(t)\sin\frac{m\pi(x-s_1)}{L}\cos\left(\frac{n\theta}{2}\right),$$
$$w=w_{mn}(t)\sin\frac{m\pi(x-s_1)}{L}\sin\left(\frac{n\theta}{2}\right), \quad (22)$$

where m and n are the numbers of half-waves along the generator and parallel circle, respectively.

In Eq. (22), if the terms of $\sin(n\theta/2)$ and $\cos(n\theta/2)$ are eliminated, the asymmetric solution is transformed into the corresponding symmetric solution.

For the sake of convenience in integration, multiplying Eqs. (18) and (19) by x and Eq. (20) by x^2, then applying the Galerkin method for the resulting equations, Eq. (18) to (20) can be developed as follows [51]:

$$\int_{s_1}^{s_2}\int_0^{2\pi}\Delta_1\cos\frac{m\pi(x-s_1)}{L}\sin\frac{n\theta}{2}x\sin\alpha\,dxd\theta=0,$$
$$\int_{s_1}^{s_2}\int_0^{2\pi}\Delta_2\sin\frac{m\pi(x-s_1)}{L}\cos\frac{n\theta}{2}x\sin\alpha\,dxd\theta=0,$$
$$\int_{s_1}^{s_2}\int_0^{2\pi}\Delta_3\sin\frac{m\pi(x-s_1)}{L}\sin\frac{n\theta}{2}x\sin\alpha\,dxd\theta$$
$$=\int_{s_1}^{s_2}\int_0^{2\pi}\rho_t\frac{\partial^2 w}{\partial t^2}\sin\frac{m\pi(x-s_1)}{L}\sin\frac{n\theta}{2}x^3\sin\alpha\,dxd\theta, \quad (23)$$

in which

$$\Delta_1=x\left[L_{11}(u)+L_{12}(v)+L_{13}(w)+L_{14}(w)\right],$$
$$\Delta_2=x\left[L_{21}(u)+L_{22}(v)+L_{23}(w)+L_{24}(w)\right],$$
$$\Delta_3=x^2\left[L_{31}(u)+L_{32}(v)+L_{33}(w)+L_{34}(w)\right]. \quad (24)$$

Substituting Eqs. (22) and (24) into Eq. (23), the following ordinary differential equations can be derived:

$$a_1\frac{d^2 w_{mn}}{dt^2}+a_2 w_{mn}+a_3 w_{mn}^2+a_4 w_{mn}^3=0, \quad (25)$$

where a_i $(i,j=1,2,3,4)$ are integral coefficients.

According to Eq. (25), the linear frequency is obtained as $\omega_L=\sqrt{a_2/a_1}$, and the nonlinear frequency can be derived as [52]:

$$\omega_{NL}=\omega_L\sqrt{1+\frac{9a_4a_2-10a_3^2}{12a_2^2}A^2}. \quad (26)$$

Here, the dimensionless vibrational amplitude A is $w_{\max}/h$, in which $w_{\max}$ is the maximum dynamic deflection.

3 RESULTS AND DISCUSSION

3.1 Comparison Studies

In this subsection, two examples are given to validate the accuracy of the present method.

Example 1. In Fig. 4, the curves of the dimensionless linear frequency λ versus the porosity coefficient e_0 for a porous FG-GRC truncated conical shell are depicted. The material properties of the matrix are $E_m=130$ GPa, $\rho_m=8960$ kg/m³ and $\mu_m=0.34$. The pattern of GPL dispersion is G–1. The material and geometrical parameters are $E_{GPL}=1.01$ TPa, $\rho_{GPL}=1062.5$ kg/m³, $\mu_{GPL}=0.86$, $a_{GPL}=2.5$ μm, $b_{GPL}=1.5$ μm, and $h_{GPL}=1.5$ nm. The geometrical parameters of the shell are $R_2/h=200\cos\alpha$, $L=s_1$ and $\alpha=10°$. The dimensionless linear frequency is $\lambda=\omega[\rho_t h^2L^2/D_1]^{0.5}$. The figure reveals that the present results are in good agreement with those given by Bahaadini et al. [38]. It is noted the natural frequency decreases with the rising porous coefficient e_0. Although both the stiffness and mass density decline with the increase of the coefficient, the decreasing speeds are different. As the decreasing speed of the mass density is higher than that of stiffness, the natural frequency reduces. In the opposite case, the natural frequency increases.

Example 2. The fundamental linear and nonlinear frequencies for an isotropic truncated conical shell surrounded by a Winkler-Pasternak foundation are calculated and listed in Table 1. The geometrical parameters of the shell are $R_1/h=300$, $L=2R_1$, $\gamma=30°$. The vibrational amplitude is $A=3$. The dimensionless frequencies are

$\Omega_L=\omega_L R_2\sqrt{(1-\mu^2)\rho/E}$, $\Omega_{NL}=\omega_{NL}R_2\sqrt{(1-\mu^2)\rho/E}$.

It is seen that the present results agree well with those given by Najafov and Sofiyev [36].

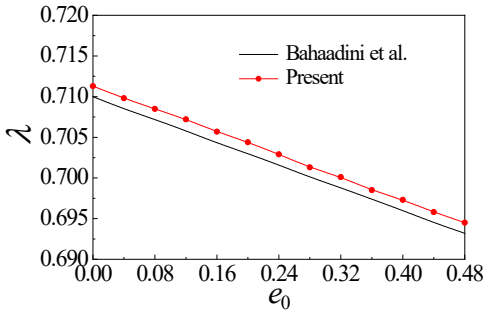

Fig. 4. *Comparison of the fundamental frequency for a porous FG truncated conical shell*

3.2 Parametric Studies

After the present method is validated, the effects of GPL, pore, and semi-vertex angle on the dimensionless linear and nonlinear frequencies for porous FG-GRC truncated conical shells surrounded by Winkler-Pasternak elastic foundations are investigated in this subsection. The material parameters of the GPL are the same as those given in Example 1. The material properties of the matrix are $E_m = 3.0$ GPa, $\rho_m = 1200$ kg/m³ and $\nu_m = 0.34$ and the geometrical parameters of the shell are $R_1/h = 100$, $L = R_1$ and $\alpha = 30°$. The dimensionless linear frequency $\varpi_L = \omega_L R_2 \sqrt{\rho_m / E_m}$. Unless specially stated, the type of the porosity distribution is P–1, and the pattern of GPL dispersion is G–1.

Table 1. *Dimensionless linear and nonlinear fundamental frequencies for an isotropic truncated conical shell rested on an elastic foundation*

k_w [N/m³]	k_p [N/m]	Ω_L		Ω_{NL}	
		Ref. [29]	Present	Ref. [29]	Present
10^5	0	0.101	0.102	0.119	0.120
	2.5×10^4	0.106	0.106	0.123	0.125
	5.0×10^4	0.110	0.111	0.126	0.128
	7.5×10^4	0.115	0.113	0.129	0.130
5.0×10^4	0	0.119	0.117	0.132	0.134
	2.5×10^4	0.123	0.123	0.138	0.140
	5.0×10^4	0.131	0.129	0.140	0.141
	7.5×10^4	0.134	0.131	0.143	0.145

The variation of the linear frequency ϖ_L with the generatrix half-wave number m and circumferential half-wave number n is shown in Fig. 5. As demonstrated by other literature [37] to [39], the number m has a different impact on the frequency with that of the genetrix number n. The frequency is raised with the rising value of m. If $n<13$, the frequency is monotonously decreased. However, if $n>13$, the frequency is increased. This is because the mass density declines more significantly than the stiffness when $n<13$. In contrast, the mass density declines more slowly than the stiffness when $n>13$. Hence, the fundamental frequency can be obtained when $m\approx1$, $n\approx13$. The following linear and nonlinear frequencies are calculated at the vibration mode (1,13).

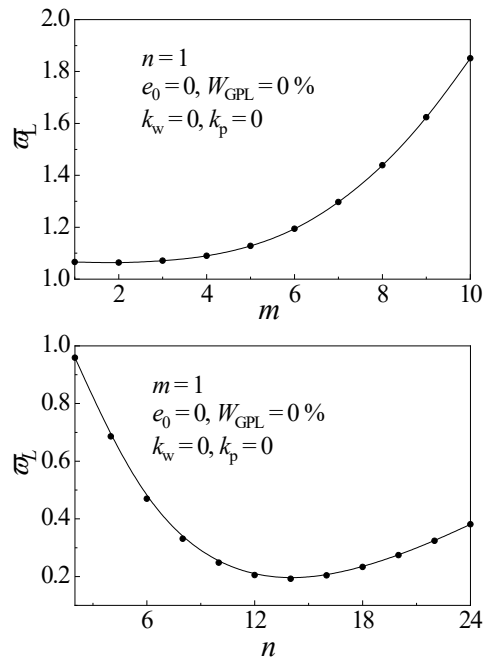

Fig. 5. *Variation of the linear frequency with a) the generatrix half-wave number m and b) the circumferential half-wave number n*

Tables 2 to 4 list the dimensionless linear frequencies ϖ_L of the shell with the different parameters of pores, GPL, and elastic foundations. Because the Winkler-Pasternak foundation can raise the effective stiffness of the conical shell, the frequency inclines with the increases of foundation parameters k_w and k_p. Furthermore, the effect of this is more significant than that of the parameter because it can enhance the effective stiffness more significantly k_w. The three tables show that the frequency increases with the increasing mass fraction of the GPLs, which is due to the fact that the elastic modulus of the GPL is higher than that of the matrix. Also, the tables reveal that the effect of the porosity coefficient e_0 is related to the parameters of the elastic foundation. If the values of k_w and k_p are not zero, the frequency reduces with the increasing value of the porosity coefficient e_0. In contrast, if the values of k_w and k_p are zero

Table 2. *Dimensionless linear frequencies ϖ_L for a porous FG-GRC conical shell distributed with G-1 GPLs and rested on an elastic foundation*

	k_w 10^6 [N/m³]	k_p 10^4 [N/m]	$e_0 = 0.0$	P-1		P-2		P-3	
				$e_0 = 0.2$	$e_0 = 0.4$	$e_0 = 0.2$	$e_0 = 0.4$	$e_0 = 0.2$	$e_0 = 0.4$
$W_{GPL} = 0.0$ %	0	0	0.192	0.188	0.184	0.185	0.178	0.196	0.192
		2.5	0.337	0.342	0.350	0.341	0.347	0.337	0.338
		5.0	0.436	0.446	0.460	0.445	0.457	0.436	0.437
	1.0	0	0.413	0.421	0.434	0.421	0.431	0.413	0.414
		2.5	0.497	0.510	0.526	0.509	0.524	0.497	0.499
		5.0	0.568	0.584	0.605	0.584	0.604	0.568	0.569
$W_{GPL} = 0.1$ %	0	0	0.231	0.226	0.221	0.223	0.213	0.231	0.230
		2.5	0.360	0.365	0.372	0.363	0.366	0.360	0.361
		5.0	0.454	0.463	0.476	0.462	0.472	0.454	0.455
	1.0	0	0.432	0.440	0.452	0.439	0.474	0.432	0.434
		2.5	0.513	0.525	0.541	0.524	0.537	0.513	0.515
		5.0	0.583	0.598	0.617	0.597	0.614	0.583	0.586
$W_{GPL} = 0.3$ %	0	0	0.294	0.289	0.283	0.284	0.271	0.294	0.293
		2.5	0.403	0.406	0.411	0.403	0.403	0.403	0.404
		5.0	0.489	0.497	0.508	0.494	0.501	0.489	0.490
	1.0	0	0.469	0.475	0.485	0.472	0.477	0.469	0.471
		2.5	0.544	0.555	0.569	0.552	0.563	0.544	0.546
		5.0	0.610	0.627	0.642	0.622	0.637	0.610	0.613

Table 3. *Dimensionless linear frequencies ϖ_L of a porous FG-GRC conical shell distributed with G-2 GPLs and rested on an elastic foundation*

	k_w 10^6 [N/m³]	k_p 10^4 [N/m]	$e_0 = 0.0$	P-1		P-2		P-3	
				$e_0 = 0.2$	$e_0 = 0.4$	$e_0 = 0.2$	$e_0 = 0.4$	$e_0 = 0.2$	$e_0 = 0.4$
$W_{GPL} = 0.1$ %	0	0	0.220	0.215	0.210	0.212	0.202	0.220	0.219
		2.5	0.353	0.358	0.364	0.356	0.360	0.353	0.354
		5.0	0.484	0.458	0.471	0.456	0.467	0.448	0.449
	1.0	0	0.426	0.434	0.446	0.433	0.442	0.426	0.426
		2.5	0.508	0.520	0.536	0.519	0.533	0.508	0.510
		5.0	0.578	0.594	0.613	0.592	0.611	0.578	0.579
$W_{GPL} = 0.3$ %	0	0	0.259	0.253	0.247	0.250	0.238	0.259	0.258
		2.5	0.379	0.382	0.387	0.380	0.382	0.379	0.380
		5.0	0.469	0.477	0.488	0.475	0.484	0.469	0.471
	1.0	0	0.480	0.455	0.465	0.453	0.460	0.448	0.449
		2.5	0.526	0.537	0.552	0.536	0.548	0.526	0.528
		5.0	0.595	0.609	0.627	0.607	0.624	0.595	0.597

Table 4. *Dimensionless linear frequencies ϖ_L of a porous FG-GPLs conical shell distributed with G-3 GPLs and rested on an elastic foundation*

	k_w 10^6 [N/m³]	k_p 10^4 [N/m]	$e_0 = 0.0$	P-1		P-2		P-3	
				$e_0 = 0.2$	$e_0 = 0.4$	$e_0 = 0.2$	$e_0 = 0.4$	$e_0 = 0.2$	$e_0 = 0.4$
$W_{GPL} = 0.1$ %	0	0	0.222	0.218	0.214	0.214	0.205	0.224	0.220
		2.5	0.369	0.374	0.382	0.372	0.377	0.368	0.370
		5.0	0.471	0.482	0.496	0.481	0.403	0.470	0.473
	1.0	0	0.427	0.436	0.448	0.434	0.444	0.426	0.429
		2.5	0.519	0.532	0.548	0.530	0.545	0.518	0.521
		5.0	0.569	0.612	0.633	0.611	0.630	0.595	0.599
$W_{GPL} = 0.3$ %	0	0	0.268	0.263	0.258	0.259	0.247	0.269	0.267
		2.5	0.398	0.402	0.409	0.399	0.402	0.397	0.399
		5.0	0.495	0.504	0.517	0.502	0.512	0.494	0.496
	1.0	0	0.453	0.460	0.471	0.458	0.465	0.452	0.454
		2.5	0.540	0.551	0.567	0.550	0.562	0.538	0.540
		5.0	0.615	0.630	0.650	0.628	0.645	0.613	0.616

(k_w=0, k_p=0), the frequency rises. Additionally, it can be observed that the effects of the pattern of GPL dispersion and the type of porosity distribution on the linear frequency can be neglected.

The influences of the type of GPL dispersion and mass fraction of the GPL on the ratio of nonlinear to linear frequency ϖ_{NL}/ϖ_L are shown in Fig. 6. Among the three patterns of GPL dispersion, the ratio for G–2 is slightly larger than those for G–3 and G–1. That is because the nonlinear frequency for G–2 increases faster than that for G–3 and G–1. Moreover, the mass fraction of the GPLs W_{GPL} rises with the increase of the ratio. For instance, when W_{GPL} changes from 0 % to 0.5 %, the ratio increases by about 9 % at A=5.

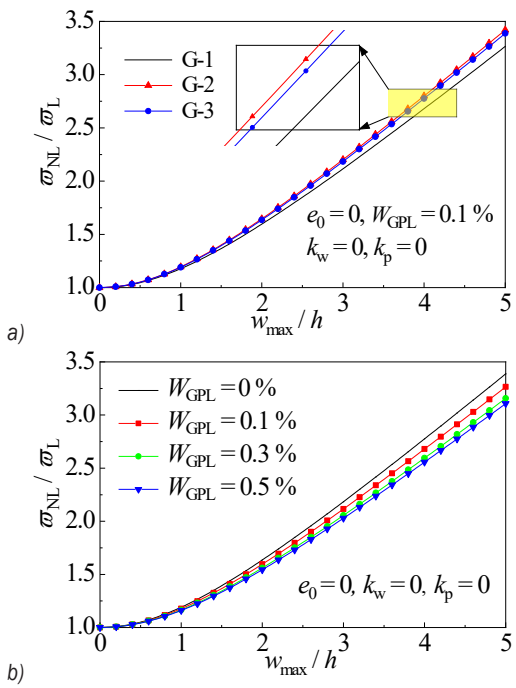

Fig. 6. *Influence of the GPLs on the frequency ratio; a) the pattern of GPL dispersion, and b) the mass fraction of the GPLs*

The influences of the porosity distribution and porosity coefficient on the frequency ratio ϖ_{NL}/ϖ_L are shown in Fig. 7. It is found that the porosity distribution has an insignificant effect on the ratio. When A = 5, the ratio for P–1 is only higher by 1.5 % than that for P–3. Also, it is found that the ratio can be raised by increasing the porosity coefficient.

Fig. 8 shows the effects of parameters k_w and k_p on the frequency ratio ϖ_{NL}/ϖ_L. It is seen that the effects are very significant. For example, when the parameter k_p changes from 0 kN/m to 75 kN/m, the ratio declines by 98.9 %.

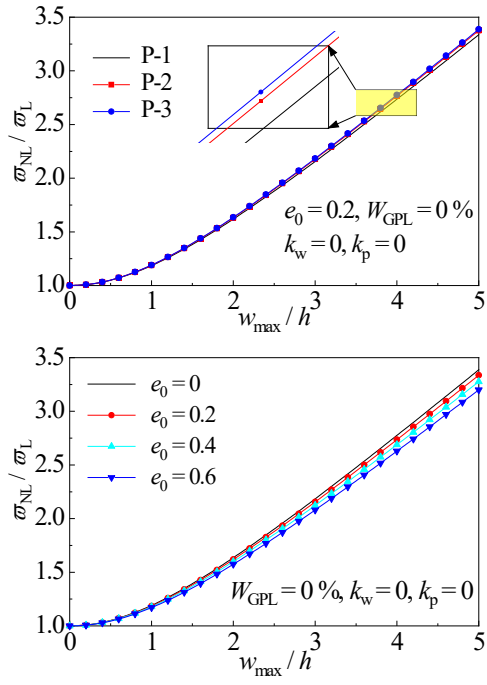

Fig. 7. *Influence of pores on the frequency ratio; a) porosity distribution, and b) porosity coefficient*

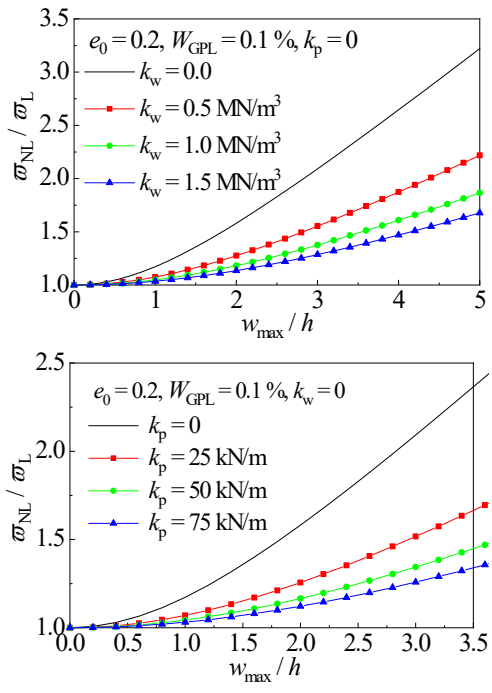

Fig. 8. *Influence of foundation parameters on the frequency ratio; a) Winkler parameter, and b) Pasternak parameter*

Finally, the effects of the semi-vertex angle α on the linear frequency ϖ_L and the ratio of linear to nonlinear frequency ϖ_{NL}/ϖ_L are shown in Fig. 9. It is shown that the linear frequency declines when the

semi-vertex angle increases. This is because the effective stiffness is raised with the increase of the semi-vertex angle. The figure also shows that the ratio reduces as the angle increases from 15º to 55º. In contrast, it is increased as the angle changes from 55º to 75º. Thus, the minimum value of frequency ratios can be obtained at $\alpha \approx 55º$.

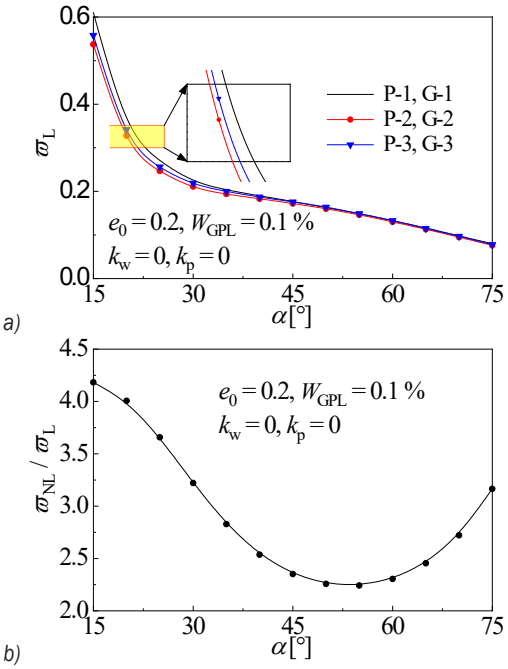

Fig. 9. *Influence of the semi-vertex angle on a) the linear frequency and b) the frequency ratio*

4 CONCLUSIONS

In this study, an improved method for evaluating the material properties of porous FG-GRCs was proposed. An analytical method to investigate the nonlinear vibration of composite such as FGM, FG-GRC, and FG-CNT porous truncated conical shells was presented. The effects of the pore, GPL, elastic foundation, and semi-vertex angle on the linear frequency and the ratio of nonlinear to linear frequency were discussed. Compared with other methods for investigating the nonlinear vibration behaviour of FG-GRC porous conical shells, the present method is simpler and briefer. However, it is not more accurate because the inertia forces $\rho_t \frac{\partial^2 u}{\partial t^2}$ and $\rho_t \frac{\partial^2 v}{\partial t^2}$ are neglected. Moreover, some interesting conclusions can be drawn from the parametric studies as follows:

1. As the values of the mass fraction of the GPLs is raised. In contrast, the frequency ratio reduces. Among the three patterns of GPLs dispersion, the frequency ratio for G-1 is the lowest, and that for G-2 is the highest.
2. The natural frequency is not monotonously varied with the rise of the porous coefficient e_0. If the mass density decreases faster than the stiffness, the natural frequency increases. In contrast, the natural frequency declines.
3. The frequency ratio can be decreased by increasing the porosity coefficient. However, the effect of porosity distribution on the frequency ratio might be negligible.
4. The linear frequency reduces if the semi-vertex angle increases. The minimum value of the frequency ratio can be obtained as the semi-vertex angle is approximately 55º.
5. Both the Winkler and Pasternak foundation parameters can significantly raise the natural frequency. However, they lower the ratio of nonlinear to linear frequency.

5 ACKNOWLEDGEMENTS

The authors thank for the financial support of the Natural Science Foundation of Guangxi [No.2021GXNSFAA220087] and the National Natural Science Foundation of China [No.12162010].

6 REFERENCES

[6] Lu, Z.Q., Yang, T.J., Brennan, M.J., Liu, Z.G., Chen, L.Q. (2017). Experimental investigation of a two-stage nonlinear vibration isolation system with high-static-low-dynamic stiffness. *Journal of Applied Mechanics*, vol. 84, no. 2, art. ID 021001, **DOI:10.1115/1.4034989**.

[7] Lu, Z.Q., Gu, D.H., Ding, H., Lacarbonara W., Chen, L.Q. (2020). Nonlinear vibration isolation via a circular ring. Mechanical Systems and Signal Processing, vol. 136, art. ID 106490, **DOI:10.1016/j.ymssp.2019.106490**.

[8] Hao, R.B., Lu, Z.Q., Ding, H., Chen, L.Q. (2022). A nonlinear vibration isolator supported on a flexible plate: analysis and experiment. *Nonlinear Dynamics*, vol. 108, p. 941-958, **DOI:10.1007/s11071-022-07243-7**.

[9] Wang, P.C., Wu, X.K., He, X.Z. (2023). Vibration-theoretic approach to vulnerability analysis of Nonlinear vehicle platoons. *IEEE Transactions on Intelligent Transportation Systems*, vol. 24, no. 10, p. 11334-11344, **DOI:10.1109/TITS.2023.3278574**.

[10] Zhou, C.H., Ren, Z.Y., Lin, Y.X., Huang, Z.H., Shi, L.W., Yang, Y., Mo, J.L. (2023). Hysteresis dynamic model of metal rubber based on higher-order nonlinear friction (HNF). *Mechanical Systems and Signal Processing*, vol. 189, art. ID 110117, **DOI:10.1016/j.ymssp.2023.110117**.

[11] Yang, Y., Kai, Y. (2023). Dynamical properties, modulation instability analysis and chaotic behaviors to the nonlinear

coupled Schrödinger equation in fiber Bragg gratings. *Modern Physics Letters B*, vol. 38, no. 6, art. ID 2350239, **DOI:10.1142/S0217984923502391**.

[12] Huang, X.L., Wang, C.Z., Wang, J.H., Wei, N.G. (2022). Nonlinear vibration analysis of functionally graded porous plates reinforced by graphene platelets on nonlinear elastic foundations. *Strojniški vestnik - Journal of Mechanical Engineering*, vol. 68, no. 9, p. 571-582, **DOI:10.5545/sv-jme.2022.274**.

[13] Chan, D.Q., Long, V.D., Duc, N.D. (2019). Nonlinear buckling and post-buckling of FGM shear-deformable truncated conical shells reinforced by FGM stiffeners. *Mechanics of Composite Materials*, vol. 54, p. 745-764, **DOI:10.1007/s11029-019-9780-x**.

[14] Chan, D.Q., Quan, T.Q., Kim, S.E., Duc, N.D. (2019). Nonlinear dynamic response and vibration of shear deformable piezoelectric functionally graded truncated conical panel in thermal environments. *European Journal of Mechanics / A Solids*, vol. 77, art. ID 103795, **DOI:10.1016/j.euromechsol.2019.103795**.

[15] Chan, D.Q., Anh, V.T.T., Duc, N.D. (2019). Vibration and nonlinear dynamic response of eccentrically stiffened functionally graded composite truncated conical shells surrounded by an elastic medium in thermal environments. *Acta Mechanics*, vol. 230, p. 157-178, **DOI:10.1007/s00707-018-2282-4**.

[16] Duc, N.D., Anh, V.T.T., Cong, P.H. (2014). Nonlinear axisymmetric response of FGM shallow spherical shells on elastic foundations under uniform external pressure and temperature. *European Journal of Mechanics A/Solids*, vol. 45, p. 80-89, **DOI:10.1016/j.euromechsol.2013.11.008**.

[17] Vuong, P.M., Duc, N.D. (2020). Nonlinear static and dynamic stability of functionally graded toroidal shell segments under axial compression. *Thin-Walled Structures*, vol. 155, art. ID 106973, **DOI:10.1016/j.tws.2020.106973**.

[18] Wang, Y.A., Sheng, Y.P., Jiang, P.C. (2019). Free vibration of graphene reinforced composite truncated conical shell. *International Journal of Mechanics Research*, vol. 8, p. 101-108, **DOI:10.12677/ijm.2019.82012**. (in Chinese)

[19] Afshari, H. (2022). Free vibration analysis of GNP-reinforced truncated conical shells with different boundary conditions. *Australian Journal of Mechanical Engineering*, vol. 20, no. 5, p. 1363-1378, **DOI:10.1080/14484846.2020.1797340**.

[20] Afshari, H. (2020). Effect of graphene nanoplatelet reinforcements on the dynamics of rotating truncated conical shells. *Journal of the Brazilian Society of Mechanical Sciences and Engineering*, vol. 42, art. ID 519, **DOI:10.1007/s40430-020-02599-6**.

[21] Damercheloo, R.A., Khorshidvand, R.A., Khorsandijou, M.S., Jabbari, M. (2021). Free vibrational characteristics of GNP-reinforced joined conical-conical shells with different boundary conditions. *Thin-Walled Structures*, vol. 169, art. ID 108287, **DOI:10.1016/j.tws.2021.108287**.

[22] Singha, D.T., Rout, M., Bandyopadhyay, T., Karmakar, A. (2021). Free vibration of rotating pretwisted FG-GRC sandwich conical shells in thermal environment using HSDT. *Composite Structures*, vol. 257, art. ID 113144, **DOI:10.1016/j.compstruct.2020.113144**.

[23] Adab, N., Arefi, M., Amabili, M. (2022). A comprehensive vibration analysis of rotating truncated sandwich conical microshells including porous core and GPL-reinforced face-sheets. *Composite Structures*, vol. 279, art. ID 114761, **DOI:10.1016/j.compstruct.2021.114761**.

[24] Adab, N., Arefi, M. (2023). Vibrational behavior of truncated conical porous GPL-reinforced sandwich micro/nano-shells. *Engineering with Computers*, vol. 39, p. 419-443, **DOI:10.1007/s00366-021-01580-8**.

[25] Yousefi, A.H., Memarzadeh, P., Afshari, H., Hosseini, J.S. (2020). Agglomeration effects on free vibration characteristics of three-phase CNT/polymer/fiber laminated truncated conical shells. *Thin-Walled Structures*, vol. 157, art. ID 107077, **DOI:10.1016/j.tws.2020.107077**.

[26] Yousefi, A.H., Memarzadeh, P., Afshari, H., Hosseini, J.S. (2023). Optimization of CNT/polymer/fiber laminated truncated conical panels for maximum fundamental frequency and minimum cost. *Mechanics Based Design of Structures and Machines*, vol. 51, no. 5, p. 3922-3944, **DOI:10.1080/15397734.2021.1945932**.

[27] Afshari, H., Amirabadi, H. (2022). Vibration characteristics of rotating truncated conical shells reinforced with agglomerated carbon nanotubes. *Journal of Vibration and Control*, vol. 28, no. 15-16, p. 1894-1914, **DOI:10.1177/10775463211000499**.

[28] Afshari, H., Ariaseresht, Y., Koloor, S.S.R., Amirabadi, H., Amirabadi, H., Bidgoli, M.O. (2022). Supersonic flutter behavior of a polymeric truncated conical shell reinforced with agglomerated CNTs. *Waves of Random Complex Media*, p. 1-25, **DOI:10.1080/17455030.2022.2082581**.

[29] Jamalabadi, M.Y.A., Borji, P., Habibi, M., Pelalak, R. (2021). Nonlinear vibration analysis of functionally graded GPL-GRC conical panels resting on elastic medium. *Thin-Walled Structures*, vol. 160, art. ID 107370, **DOI:10.1016/j.tws.2020.107370**.

[30] Ansari, R., Hassani, R., Hasrati, E., Rouhi, H. (2022). Studying nonlinear vibrations of composite conical panels with arbitrary-shaped cutout reinforced with graphene nanoplatelets based on higher-order shear deformation theory. *Journal of Vibration and Control*, vol. 28, no. 21-22, p. 3019-3041, **DOI:10.1177/10775463211024847**.

[31] Yang, S.W., Hao, Y.X., Zhang, W., Yang, L., Liu, L.T. (2021). Nonlinear vibration of functionally graded graphene platelet reinforced composite truncated conical shell using first-order shear deformation theory. *Applied Mathematics and Mechanics (English Edition)*, vol. 42, p. 981-998, **DOI:10.1007/s10483-021-2747-9**.

[32] Wang, A.W., Pang, Y.Q., Zhang, W., Jiang, P.C. (2019). Nonlinear dynamic analysis of functionally graded graphene reinforced composite truncated conical shells. *International Journal of Bifurcation and Chaos*, vol. 29, no. 11, p. 12244-12252, **DOI:10.1142/S0218127419501487**.

[33] Ding, H.X., She, G.L. (2023). Nonlinear primary resonance behavior of graphene platelet reinforced metal foams conical shells under axial motion. *Nonlinear Dynamics*, vol. 111, p. 13723-13752, **DOI:10.1007/s11071-023-08564-x**.

[34] Bidgoli, E.M.R., Arefi, M. (2023). Nonlinear vibration analysis of sandwich plates with honeycomb core and graphene nanoplatelet-reinforced face-sheets. *Archives of Civil and*

Mechanical Engineering, vol. 23, art. ID. 56, **DOI:10.1007/s43452-022-00589-0**.

[35] Wu, H.L., Yang, J., Kitipornchai, S. (2020). Mechanical analysis of functionally graded porous structures: A review. *International Journal of Structural Stability and Dynamics*, vol. 20, no. 13, art. ID 2041015, **DOI:10.1142/S0219455420410151**.

[36] Li, H., Hao, Y.X., Zhang, W., Liu, L.T., Yang, S.W., Wang, D.M. (2021). Vibration analysis of porous metal foam truncated conical shells with general boundary conditions using GDQ. *Composite Structures*, vol. 269, art. ID 114036, **DOI:10.1016/j.compstruct.2021.114036**.

[37] Amirabadi, H., Afshari, H., Afjaei, M.A., Sarafeaz, M. (2022). Effect of variable thickness on the aeroelastic stability boundaries of truncated conical shells. *Waves of Random Complex Media*, **DOI:10.1080/17455030.2022.2157517**.

[38] Mohammadrezazadeh, S., Jafari, A.A. (2022). The study of the nonlinear vibration of S-S and C-C laminated composite conical shells on elastic foundations through an approximate method. *Proceedings of the Institution of Mechanical Engineers, Part C: Journal of Mechanical Engineering Science*, vol. 236, no. 3, p. 1377-1390, **DOI:10.1177/09544062211021439**.

[39] Hao, X.Y., Li, H., Zhang, W., Ge, X.S., Yang, W.S., Cao, Y.T. (2022). Active vibration control of smart porous conical shell with elastic boundary under impact loadings using GDQM and IQM. *Thin-Walled Structures*, vol. 175, art. ID 109232, **DOI:10.1016/j.tws.2022.109232**.

[40] Chan, D.Q., Thanh, N.T., Khoa, N.K., Duc, N.D. (2020). Nonlinear dynamic analysis of piezoelectric functionally graded porous truncated conical panel in thermal environments. *Thin-Walled Structures*, vol. 154, art. ID 106837, **DOI:10.1016/j.tws.2020.106837**.

[41] Huang, X.L., Wang, J.H. Wei, N.G., Wang, C.Z., Bin, M. (2023). Buckling and vibration of porous sigmoid functionally graded conical shells. *Journal of Theoretical and Applied Mechanics*, vol. 61, p. 559-570, **DOI:10.15632/jtam-pl/168072**.

[42] Kiarasi, F., Babaei, B., Sarvi, P., Asemi, K., Hosseini, M., Bidgol, M.O. (2021). A review on functionally graded porous structures reinforced by graphene platelets. *Journal of Computational Applied Mechanics*, vol. 52, no. 4, p. 731-750, **DOI:10.22059/jcamech.2021.335739.675.**

[43] Bahhadini, R., Saidi, A.R., Arabjamaloei, Z., Chanbari-Nejad-Parizi, A. (2019). Vibration analysis of functionally graded graphene reinforced porous nanocomposite shells. *International Journal of Applied Mechanics*, vol. 11, no. 7, art. ID 1950068, **DOI:10.1142/S1758825119500686**.

[44] Yan, K., Zhang, Y., Cai, H., Tahouneh, V. (2020). Vibrational characteristic of FG porous conical shells using Donnell's shell theory. *Steel and Composite Structures*, vol. 35, no. 2, p. 249-260, **DOI:10.12989/scs.2020.35.2.249**.

[45] Rahmani, M., Mohammadi, Y., Kakavand, F. (2019). Vibration analysis of sandwich truncated conical shells with porous FG face sheets in various thermal surroundings. *Steel and Composite Structures*, vol. 32, no. 2, p. 239-252, **DOI:10.12989/scs.2019.32.2.239**.

[46] Esfahani, M.N., Hashemian, M., Aghadavoudi, F. (2022). The vibration study of a sandwich conical shell with a saturated FGP core. *Scientific Reports*, vol. 12, art. ID 4950, **DOI:10.1038/S41598-022-09043-W**.

[47] Cuong-Le T., Nguyen, K.D., Nguyen-Trong, N., Khatir, S., Nguyen-Xuan, H., Abdel-Wahab, M. (2021). A three-dimensional solution for free vibration and buckling of annular plate, conical, cylinder and cylindrical shell of FG porous-cellular materials using IGA. *Composite Structures*, vol. 259, art. ID 113216, **DOI:10.1016/j.compstruct.2020.113216**.

[48] Sobhani, E., Arbabian, A., Civalek, Ö., Avcar, M. (2022). The free vibration analysis of hybrid porous nanocomposite joined hemispherical-cylindrical-conical shells. *Engineering with Computers*, vol. 38, p. 3125-3152, **DOI:10.1007/s00366-021-01453-0**.

[49] Kiarasi, F., Babaei, M., Mollaei, S., Mohammadi, M., Asemi, K. (2021). Free vibration analysis of porous FG joined truncated conical-cylindrical shell reinforced by graphene nanoplatelets. *Advances in Nano Research*, vol. 11, no. 4, p. 361-380, **DOI:10.12989/anr.2021.11.4.361**.

[50] Sofieyev, A.H., Kuruoglu, N. (2011). Natural frequency of laminated orthotropic shells with different boundary conditions and resting on the Pasternak type elastic foundation. *Composites Part B: Engineering*, vol. 42, no. 6, p. 1562-1570, **DOI:10.1016/j.compositesb.2011.04.015**.

[51] Fu, T., Wu, X., Xiao, Z.M., Chen, A.B., Li, B. (2021). Analysis of vibration characteristics of FGM sandwich joined conical-conical shells surrounded by elastic foundations. *Thin-Walled Structures*, vol. 165, art. ID 107979, **DOI:10.1016/j.tws.2021.107979**.

[52] Deniz, A., Zerin, Z., Karaca, Z. (2016). Winkler-Pasternak foundation effect on the frequency parameter of FGM truncated conical shells in the framework of shear deformation theory. *Composites Part B: Engineering*, vol. 104, p. 57-70, **DOI:10.1016/j.compositesb.2016.08.006**.

[53] Safarpour, M., Rahimi, A.R., Alibeigloo, A. (2020). Static and free vibration analysis of graphene nanoplatelets reinforced composite truncated conical shell, cylindrical shell, and annular plate using theory of elasticity and DQM. *Mechanics Based Design of Structures and Machines*, vol. 48, no. 4, p. 496-524, **DOI:10.1080/15397734.2019.1646137**.

[54] Eyvazian, A., Musharavati, F., Tarlochan, F., Pasharavesh, A., Rajak, D.K., Husain, M.B., Tran, T.N. (2020). Free vibration of FG-GPLRC conical panel on elastic foundation. *Structural Engineering and Mechanics*, vol. 75, no. 1, p. 1-18, **DOI:10.12989/sem.2020.75.1.001**.

[55] Amirabadi, H., Farhatnia, F., Civalek, O. (2021). Frequency response of rotating two-directional functionally graded GPL-reinforced conical shells on elastic foundation. *Journal of the Brazilian Society of Mechanical Sciences and Engineering*, vol. 43, art. ID 349, **DOI:10.1007/s40430-021-03058-6**.

[56] Duc, N.D., Cong, P.H., Tuan, N.D., Tran, P., Thanh, N.V. (2017). Thermal and mechanical stability of functionally graded carbon nanotubes (FG CNT)-reinforced composite truncated conical shells surrounded by the elastic foundations. *Thin-Walled Structures*, vol. 115, p. 300-310, **DOI:10.1016/j.tws.2017.02.016**.

[57] Huang, X.L., Shen, H.S. (2004). Nonlinear vibration and dynamic response of functionally graded plates in thermal environments. *International Journal of Solids and Structures*, vol. 41, no. 9-10, p. 2403-2427, **DOI:10.1016/j.ijsolstr.2003.11.012**.

7 APPENDIX

$$L_{14}(w)=A_{11}x\frac{\partial w}{\partial x}\frac{\partial^2 w}{\partial x^2}-\frac{A_{12}+A_{22}}{2x^2\sin^2\alpha}\left(\frac{\partial w}{\partial\theta}\right)^2+\frac{A_{12}+A_{66}}{x\sin^2\alpha}\frac{\partial w}{\partial\theta}\frac{\partial^2 w}{\partial x\partial\theta}+A_{66}\frac{1}{x\sin^2\alpha}\frac{\partial w}{\partial x}\frac{\partial^2 w}{\partial\theta^2}+\frac{1}{2}\left(A_{11}-A_{22}\right)\left(\frac{\partial w}{\partial x}\right)^2,$$

$$L_{24}(w)=\left(A_{12}+A_{66}\right)\frac{1}{\sin\alpha}\frac{\partial w}{\partial x}\frac{\partial^2 w}{\partial x\partial\theta}+A_{22}\frac{1}{x^2\sin^3\alpha}\frac{\partial w}{\partial\theta}\frac{\partial^2 w}{\partial\theta^2}+A_{66}\frac{1}{x\sin\alpha}\frac{\partial w}{\partial x}\frac{\partial w}{\partial\theta}+A_{66}\frac{1}{\sin\alpha}\frac{\partial^2 w}{\partial x^2}\frac{\partial w}{\partial\theta},$$

$$\begin{aligned}L_{34}(u,v,w)=&\left(B_{11}-3B_{12}\right)\frac{\partial w}{\partial x}\frac{\partial^2 w}{\partial x^2}+\left(B_{12}-B_{22}+2B_{66}\right)\frac{1}{x^2\sin^2\alpha}\frac{\partial w}{\partial x}\frac{\partial^2 w}{\partial\theta^2}+\left(A_{12}-\frac{1}{2}A_{22}\right)\cot\alpha\left(\frac{\partial w}{\partial x}\right)^2+A_{12}\cot\alpha\, w\frac{\partial^2 w}{\partial x^2}\\&+2\left(B_{66}-B_{12}\right)\frac{1}{x\sin^2\alpha}\frac{\partial^2 w}{\partial x^2}\frac{\partial^2 w}{\partial\theta^2}+2\left(4B_{66}-B_{12}\right)\frac{1}{x^2\sin^2\alpha}\frac{\partial w}{\partial\theta}\frac{\partial^2 w}{\partial x\partial\theta}+B_{12}\frac{1}{x\sin^2\alpha}\frac{\partial w}{\partial\theta}\frac{\partial^3 w}{\partial x^2\partial\theta}\\&+\left(B_{12}+B_{22}-4B_{66}-\frac{1}{2}A_{22}x\cot\alpha\right)\frac{1}{x^3\sin^2\alpha}\left(\frac{\partial w}{\partial\theta}\right)^2+A_{22}\cot\alpha\frac{1}{x^2\sin^2\alpha}w\frac{\partial^2 w}{\partial\theta^2}+B_{22}\frac{1}{x^3\sin^4\alpha}\frac{\partial w}{\partial\theta}\frac{\partial^3 w}{\partial\theta^3}\\&-2B_{66}\frac{1}{x^2\sin^3\alpha}\frac{\partial w}{\partial\theta}\frac{\partial^3 w}{\partial x\partial\theta^2}-A_{12}\frac{1}{x^2\sin^2\alpha}\frac{\partial w}{\partial x}\left(\frac{\partial w}{\partial\theta}\right)^2+A_{12}\frac{1}{x\sin^2\alpha}\frac{\partial w}{\partial x}\frac{\partial w}{\partial\theta}\frac{\partial^2 w}{\partial x\partial\theta}+\frac{1}{2}A_{11}x\frac{\partial^2 w}{\partial x^2}\left(\frac{\partial w}{\partial x}\right)^2\\&+\frac{1}{2}A_{12}\frac{1}{x\sin^2\alpha}\frac{\partial^2 w}{\partial x^2}\left(\frac{\partial w}{\partial\theta}\right)^2-A_{66}\frac{1}{x^2\sin^2\alpha}\frac{\partial w}{\partial x}\left(\frac{\partial w}{\partial\theta}\right)^2+A_{66}\frac{1}{x\sin^2\alpha}\frac{\partial^2 w}{\partial x^2}\left(\frac{\partial w}{\partial\theta}\right)^2+4A_{66}\frac{1}{x\sin^2\alpha}\frac{\partial w}{\partial\theta}\frac{\partial w}{\partial x}\frac{\partial^2 w}{\partial x\partial\theta}\\&+A_{66}\frac{1}{x\sin^2\alpha}\frac{\partial^2 w}{\partial\theta^2}\left(\frac{\partial w}{\partial x}\right)^2+A_{66}\frac{1}{x^2\sin^3\alpha}\frac{\partial^2 w}{\partial x\partial\theta}\left(\frac{\partial w}{\partial\theta}\right)^2+A_{66}\frac{1}{x\sin^3\alpha}\frac{\partial w}{\partial x}\frac{\partial w}{\partial\theta}\frac{\partial^2 w}{\partial\theta^2}+\frac{1}{2}A_{12}\frac{1}{x\sin^2\alpha}\frac{\partial^2 w}{\partial\theta^2}\left(\frac{\partial w}{\partial x}\right)^2\\&+\frac{1}{2}A_{22}\frac{1}{x^3\sin^4\alpha}\frac{\partial^2 w}{\partial\theta^2}\left(\frac{\partial w}{\partial\theta}\right)^2+A_{11}\frac{\partial w}{\partial x}\frac{\partial u}{\partial x}+A_{11}x\frac{\partial w}{\partial x}\frac{\partial^2 u}{\partial x^2}+A_{12}\frac{1}{\sin\alpha}\frac{\partial w}{\partial x}\frac{\partial^2 v}{\partial x\partial\theta}+A_{12}\frac{\partial w}{\partial x}\frac{\partial u}{\partial x}+A_{11}x\frac{\partial^2 w}{\partial x^2}\frac{\partial u}{\partial x}\\&+A_{12}\frac{1}{\sin\alpha}\frac{\partial^2 w}{\partial x^2}\frac{\partial v}{\partial\theta}+A_{12}u\frac{\partial^2 w}{\partial x^2}-A_{66}\frac{1}{\sin\alpha}\frac{\partial w}{\partial\theta}\frac{\partial u}{\partial\theta}+A_{66}\frac{1}{x\sin^2\alpha}\frac{\partial w}{\partial\theta}\frac{\partial^2 u}{\partial x\partial\theta}+A_{66}\frac{1}{x^2\sin\alpha}\frac{\partial w}{\partial\theta}v-A_{66}\frac{1}{x\sin\alpha}\frac{\partial w}{\partial\theta}\frac{\partial v}{\partial x}\\&+A_{66}\frac{1}{\sin\alpha}\frac{\partial w}{\partial\theta}\frac{\partial^2 v}{\partial x^2}+A_{66}\frac{1}{x\sin^2\alpha}\frac{\partial^2 w}{\partial x\partial\theta}\frac{\partial u}{\partial\theta}-A_{66}\frac{1}{x\sin\alpha}v\frac{\partial^2 w}{\partial x\partial\theta}+A_{66}\frac{1}{\sin\alpha}\frac{\partial^2 w}{\partial x\partial\theta}\frac{\partial v}{\partial x}+A_{66}\frac{1}{x\sin^2\alpha}\frac{\partial w}{\partial x}\frac{\partial^2 u}{\partial\theta^2}\\&-A_{66}\frac{1}{x\sin\alpha}\frac{\partial w}{\partial x}\frac{\partial v}{\partial\theta}+A_{66}\frac{1}{\sin\alpha}\frac{\partial w}{\partial x}\frac{\partial^2 v}{\partial x\partial\theta}+A_{66}\frac{1}{x\sin^2\alpha}\frac{\partial^2 w}{\partial x\partial\theta}\frac{\partial u}{\partial\theta}-A_{66}\frac{1}{x\sin\alpha}\frac{\partial^2 w}{\partial x\partial\theta}v+A_{66}\frac{1}{\sin\alpha}\frac{\partial^2 w}{\partial x\partial\theta}\frac{\partial v}{\partial x}\\&+A_{66}\frac{1}{x^2\sin^3\alpha}\frac{\partial w}{\partial\theta}\frac{\partial^2 u}{\partial\theta^2}-A_{66}\frac{1}{x^2\sin^2\alpha}\frac{\partial w}{\partial\theta}\frac{\partial v}{\partial\theta}+A_{66}\frac{1}{x\sin^2\alpha}\frac{\partial^2 v}{\partial x\partial\theta}\frac{\partial w}{\partial\theta}+A_{12}\frac{1}{x\sin^2\alpha}\frac{\partial^2 w}{\partial\theta^2}\frac{\partial u}{\partial x}\\&+A_{22}\frac{1}{x^2\sin^3\alpha}\frac{\partial^2 w}{\partial\theta^2}\frac{\partial v}{\partial\theta}+A_{22}\frac{1}{x^2\sin^2\alpha}\frac{\partial^2 w}{\partial\theta^2}u\end{aligned}$$